Fracture Stability Assessment during SAGD operations using 4D Geomechanical Models

Marc Holland, Wouter van der Zee

Baker Hughes, Reservoir Technology and Software

Abstract*: In the oil and gas industry, steam assisted gravity drainage (SAGD) is an operation where steam is injected into a reservoir to lower the viscosity of heavy oil to allow its production. The injection of steam leads to thermally induced stresses and pore pressure changes in the reservoir and its proximity. Although the pressure and temperature evolution can be modelled with reservoir simulators, they neglect the change of the stress field in relation to these properties, which can impact the stability of faults and fractures. These active faults and fractures, in turn, affect the fluid transport properties. In order to assess the potential for fault and fracture (re-)activation we created a model of a SAGD operation by coupling the outcome of a reservoir simulation to a 4D geomechanical finite-element model using Abaqus. The stresses calculated in the Abaqus model are used as the input for our fracture stability calculations. First, a conservative analysis uses a directionless assessment without the need for discrete fracture and fault orientations. It shows extensive critically-stressed regions above and below the injection well, which extend into the cap rock. A second analysis using the available fault models reveals that the bounding faults have critically stressed patches toward the end of the stimulation. Quantitative risk assessment is performed to investigate the influence of a range of input parameters on the fault stability and to quantify the risk of fault reactivation. The outcome of the study stresses the need for a detailed discussion of the cap rock thickness and the impact of potential of fractures.*

Keywords*: Oil and Gas, Geomechanics, Steam Assisted Gravity Drainage, SAGD, Reservoir, Thermal Expansion, , Abaqus, JewelSuite, , Stress, Displacement, Permeability, Cap Rock, Seal integrity, Faults, Fractures, Stability, Critically Stressed, Reactivation*

1. Background

The choice of how to produce hydrocarbons from the subsurface depends on a variety of circumstances. For shallow reservoirs holding hydrocarbons which are too viscous to be produced economically with conventional means, a technique can be applied which is called “steam assisted gravity drainage” or SAGD (Butler, 1991). Here the viscosity of the hydrocarbons is reduced by locally increasing the rock temperature with the injection of hot steam. For this operation typically two sub-horizontal wells, parallel in the vertical plane, are drilled. In the upper well steam is injected over a prolonged time. Through convection and conduction the rock surrounding the well is heated and the elevated temperatures mobilize the hydrocarbons which are then produced from the lower well. The operational parameters for SAGD need to be constrained to honor both economic as well as physical limits. The economic limits are primarily based on technical expenses such as the cost of surface equipment and the cost of prolonged steam injection. Physical limits on the other hand are primarily linked to the safety of the operation, where the containment of the steam inside the reservoir is of prime importance. The injected steam is confined in the reservoir by the same sealing elements which are responsible for the accumulation and containment of hydrocarbons over geological time scales. Seals may be created by bounding faults which may act as lateral flow barriers, as well as “cap-rock” which is impermeable and acts as a vertical flow barrier. The integrity of these sealing elements needs to be maintained during the injection of steam to avoid leakage of steam and hydrocarbons into shallower layers, the aquifer, or even to the surface (ERCB, 2010; ERCB, 2013). A compromised seal may thus impose serious health, safety and environmental threats.

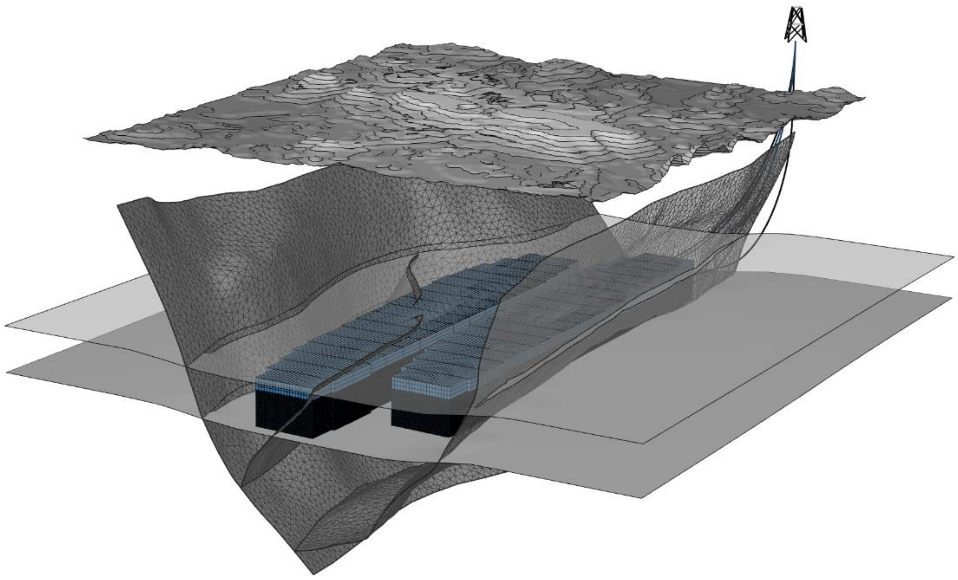

Figure 1 – The SAGD model represents a shallow reservoir at approximately 280 m depth. The reservoir layer is approximately 70 m thick as defined by the two horizons and is laterally bound by the two major fault surfaces. A third small fault is presumed to be present inside the reservoir. These model elements are represented by triangulated surfaces. Other objects include well bores for the injection and production as well as two reservoir grids (blue) in which the injection of the steam and production of the hydrocarbons are modelled. The contoured horizon at the top describes the surface topography.

In order to assess the operational parameters and minimize the risk of losing the seal integrity we combine the outcome of a reservoir simulation with a geomechanical simulation carried out in Abaqus. Here, the temperature and pore pressure evolution of the reservoir section are fed into a mechanical simulation of the subsurface system to solve for the evolution of the effective stresses. These results are then used to assess the likelihood of causing fracture slip, which could compromise the seal integrity. This workflow is demonstrated in a shallow reservoir undergoing SAGD as illustrated in Figure 1. Here, a reservoir compartment of approximately 70 m thickness is located at a shallow depth of approximately 280 m. The reservoir layer is laterally bound by two normal, low-offset faults. In this reservoir two SAGD operations are carried out where steam is injected into two sites simultaneously over a prolonged period. The increase in the rock temperature at these sites is locally more than 250°Celsius.

2. Pre-processing and geomechanical simulation

To assess the risk of fracture activation or seal breach, an integrated approach is necessary in which different simulation techniques and grids need to be combined. As previously mentioned, the input for the geomechanical simulation is partly taken from the reservoir simulations. The reservoir model is a purpose-made fluid flow simulation, typically carried out to constrain the economic limits. Using a finite-difference approach, the thermal and pressure evolution of the reservoir layer is modelled using both injection and production. The reservoir simulation considers the chemical composition of the hydrocarbons, the associated phase changes and hydrocarbon saturations. The reservoir grids typically are layer conforming. Grid cells are commonly IJK organized hexahedral cells with high length to height ratios so they better replicate the flow properties imposed by geological layering.

To integrate the data we use the sub-surface modelling platform JewelSuite ™ in which the reservoir models are loaded along with supporting structural elements (faults, horizons, topography) and well data. Two reservoir simulation grids are present in which the temperature and pressure evolution of the SAGD operation were modelled. These reservoir grids each have about 40 thousand grid cells (33×17×73 elements in IJK), holding in total 80 reported time steps. These highly-specialized simulations cover only the reservoir section and are laterally confined as the changes in temperature and pressure are believed to act locally. The geomechanical simulation of the stress evolution is carried out with Abaqus. In order to link these simulations, several pre- and post-processing steps are necessary, which are described below in more detail.

The sub-surface stress state in the reservoir is dependent not only on the pressure and temperature evolution as calculated by the reservoir simulation but it is a function of a much larger system. The contribution of the vertical load of the overburden for example requires the geomechanical model to be extended upwards to the topographic surface. Effects related to the stiffness of the rock layers require not only the knowledge of the elastic parameters throughout the model, but also require the model to be extended laterally ("sideburden") and downwards ("underburden"). In order to capture these influences and to avoid artifacts from the model boundary, the mesh for the geomechanical model covers a vertical column from the surface to about twice the depth of interest (>560 m) and has lateral dimensions of at least three times the size of the area of interest in which the steam injection is conducted. The geomechanical simulation therefore covers a much larger volume compared to the reservoir simulation. As property data and the supporting structural elements are typically missing outside the volume of interest, user interaction and user decisions are required to construct a large enough property volume for the geomechanical simulation. The triangulated surfaces available for topography, faults and horizons are thus extended outwards and the geological grid is constrained by these extended surfaces. This geological grid honors the structural constraints and incorporates available formation top data from well-based interpretations. The purpose of using a geological, layer-conforming grid is to replicate the geological layering to assist in the population of geomechanical properties. The required properties for the simulation are density, the elastic properties Young's modulus and Poisson's ratio as well as the ambient stresses, pore pressure and information on the thermal expansion coefficient. These properties are typically modelled based on the well log data to form a verified well-centric 1D geomechanical model. The 1D data is then extrapolated from the wells into the 3D geological grid to form a 3D property container. Details on these two workflow steps are beyond the scope of this paper, but see e.g.: Holland et al. (2010) or Zoback (2007).

The constraints for the mesh for the geomechanical simulation are prepared in the JewelSuite™ subsurface modeling software. The triangulated surfaces of the structural elements are re-meshed in such a way that a "water-tight" structural model is created. As the triangulated surfaces are used as mesh seeding points in Abaqus, we use the triangle size on the surfaces to enforce a meshing gradient. The Abaqus mesh is constructed from tetrahedrons. As the replication of thin but laterally extensive layers with tetrahedrons is computationally expensive, we only use high resolution tetrahedrons in the central volume of interest and gradually increase the element size outwards (van der Zee, et al., 2011). The "coarsening step" of enforcing a gradual increase of triangle size is performed in the subsurface modeling software to ensure quality control and ease of interaction with the original objects. The meshing of the geomechanical simulation grid is performed in Abaqus/CAE using a data exchange through the Python™ interface. Details of the meshing procedure can be found in van der Zee et al. (2011). Upon successful creation, the mesh is subsequently imported and visualized in the subsurface modeling software. If necessary, poor elements can be identified in the mesh and the triangulated surfaces can be modified accordingly for another meshing run. In the presented scenario the geomechanical model is built with three reservoir faults and a few structural horizons. Grid or mesh refinement is done closer to the well trajectories for a high resolution in the volume of interest. The created finite element mesh consists of 809,000 C3D10MP elements (Figure 2).

We did not implement the faults as sliding surfaces (e.g. contact modeling) in the analysis because the slip of such a contact would alter the stress field. Although modeling such behavior may be more accurate, the purpose of the analysis is not to model the consequences of fault slip but to assess the risk of slip initiation. The faults are included as geometric features in the mesh where the absence of slip provides stress continuity, which allows us to conservatively assess the risk of slip. This is required as the faults' properties and the faults' orientations are not precisely known. We assess the risks and uncertainties behind these assumptions below, using dedicated analytical geomechanical techniques (see Post-processing and results).

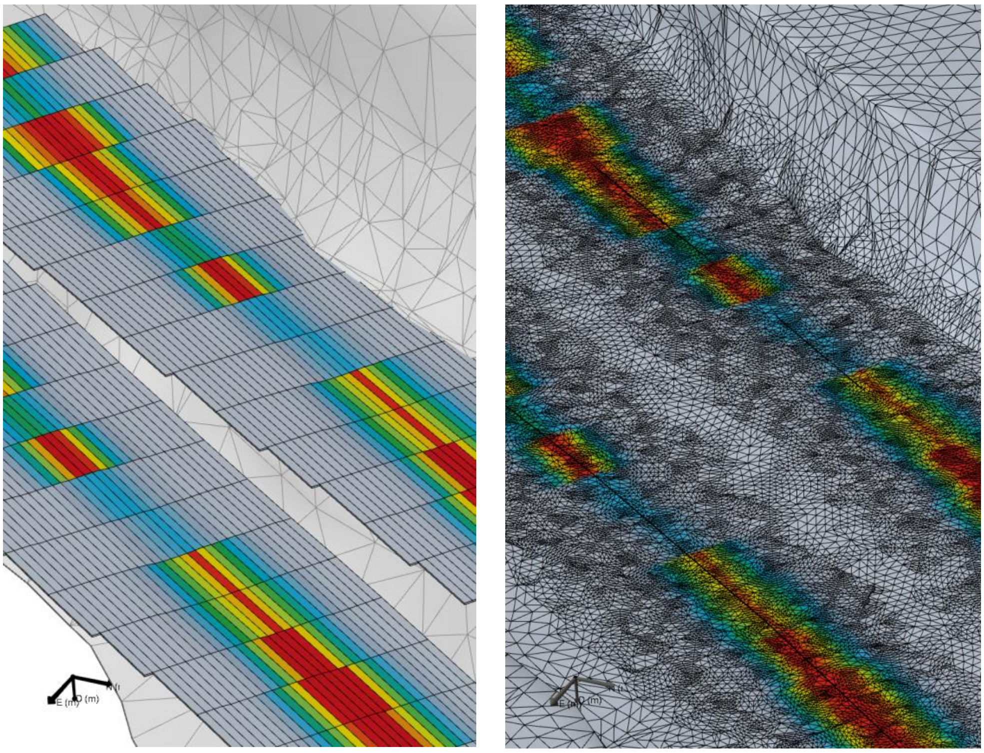

Figure 2 – A k-slice from the two reservoir simulation grids (left) and the same slice through the 3D mesh used for the geomechanical simulation (right). Both images use temperature for the color coding.

The Abaqus input file for the geomechanical analysis is created fully using the JewelSuite™ software. Using the mapping capabilities and the unit management system of the software, some material properties are mapped (e.g., temperature, Figure 2) from the 3D geological grid onto the 3D mesh and provided as field variables where the Abaqus material properties in the mesh are made dependent on these field variables. Other material properties are defined per element set (Table 1). The mesh for the finite element simulation consists of C3D10MP elements and a linear poro-elastic material model. The necessary boundary conditions for the simulation are derived from the regional geological stress field as present in the 1D geomechanical models.

After an initialization step to obtain a stress state which is in equilibrium with the input parameters (e.g. density and gravitational load, see van der Zee et al., 2011), the changing pore pressure and temperatures are applied to the model. The pore pressure field is applied as changing boundary conditions (d.o.f. 8) at every node in the model. The temperature field of the reservoir models (as present in the 3D geological grid) is applied using the *Temperature option on the nodes with changing temperatures.

The created input file is then submitted to Abaqus/Standard for calculation. From the 80 reported time steps of the reservoir simulation, every 2nd step was used in the geomechanical simulation. Upon completion the results are read back into the JewelSuite™ subsurface modeling software for post-processing in the geological context.

3. Post-processing and results

During the post-processing step we assess fault stability using a dedicated geomechanical model in the JewelSuite™ subsurface modeling software. The full stress tensor and pore pressure obtained from the finite element simulation are used for the geomechanical analysis, and a Mohr-Coulomb failure criterion is used as the basis for determining whether faults may have slipped. In this step, we focus on the re-activation of preexisting fault and fracture planes. The effective normal stress and shear stress component on each plane is calculated based on the fracture orientation and the surrounding stress field (Chou & Pagano, 1967). Assuming no cohesion (because the faults and fractures already exist) and a sliding friction coefficient of 0.6 (Byerlee, 1978) we calculate the ratio of the critical shear stress to the actual shear stress. This measure is called Tau Ratio (van der Zee, et al., 2014). Values of Tau Ratio close to 1.0 or above are considered to be critically stressed, where the fracture is at risk of slipping. Due to asperities on the fracture planes, slip would create openings along the fracture plane and thus increase the fracture's permeability (Barton & Zoback, 1995). Critically stressed fractures or faults therefore may pose a risk of compromising seal integrity.

There are significant uncertainties in determining fault and fracture orientations, locations, and densities. First, the faults which are to be tested in the analysis are commonly interpreted from subsurface seismic data. These data sets may have a considerable spatial uncertainty and a coarse resolution making it difficult to provide accurate interpretations. Small-scale undulations of the fault plane may be unresolvable, leaving the analysis biased toward the average orientation of the faults. Second, smaller scale fractures are not visible at all on sub-surface seismic as they fall below the resolution of the measurements. However, since fractures are extremely common in all rock, their potential contribution to the risk should be assessed.

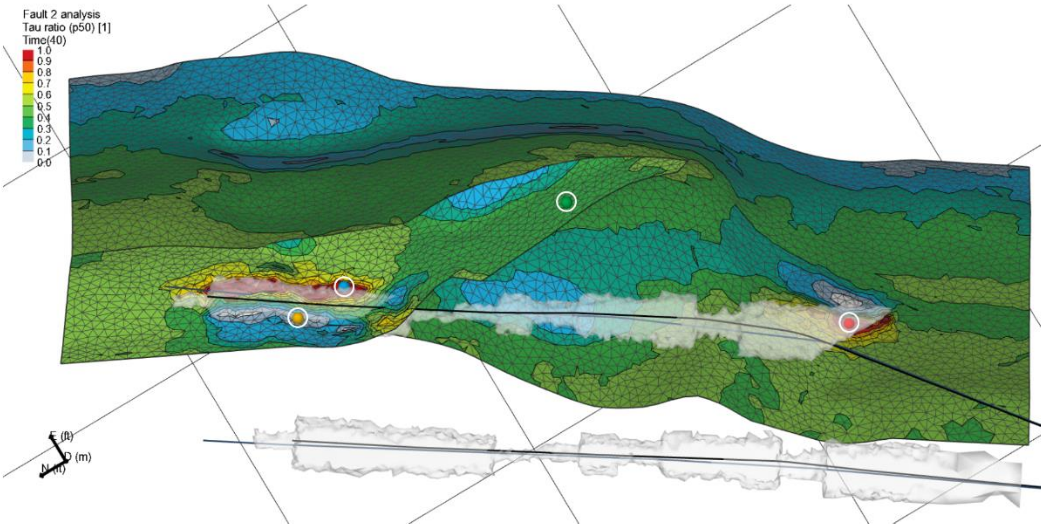

Figure 3 – Top view of two of the reservoir faults. The faults are color-coded for Tau Ratio (P50) at the final step of the analysis. Red colors indicate critically stressed sections of the fault. The four marked points indicate locations on the fault on which the time series for the P10, P50 and P90 values of Tau ratio are sampled, shown in Figure 4. The blue and red spheres are showing critically stressed sections on the fault. The green and yellow spheres show non-critical sections. The temperature body of the steam injection is rendered semi-transparent for reference.

We map the stress field from the 3D mesh onto the nodes of the triangulated fault surfaces to calculate the fault slip risk of the bounding faults. Rather than calculate only one pair of shear and effective normal stress values for every single node (Holland, 2015), we perform 1,000 Monte Carlo simulations at each node to incorporate the model uncertainties. We believe that such an uncertainty assessment would be too time consuming in Abaqus, and therefore decided to run multiple analyses on the results in JewelSuite™. At each node, some the original input parameters are altered by random offsets using Gaussian distributions. The pore pressure is allowed to be changed with a standard deviation of 0.1 MPa, the dip angle by a standard deviation of 10.0 degrees, the azimuth of the dip direction by 5.0 degrees and the sliding friction coefficient by 0.05. From these 1,000 realizations for every node, the results are sorted and only the P10, P50 and P90 results stored on the triangulated surfaces (Figure 3). Figure 4 shows a plot in which the time series of Tau Ratio is presented at the four locations indicated in Figure 3.

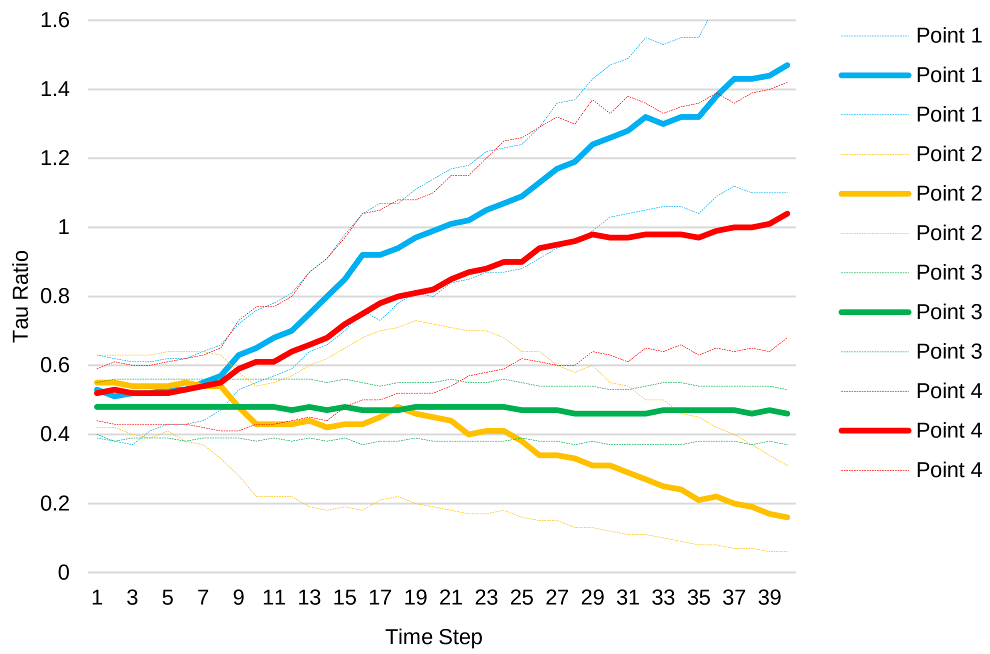

Figure 4 – Time series for the Monte Carlo simulation of Tau Ratio at four selected locations shown on the fault in Figure 3. Both the blue and red curves exceed the critical limit of 1.0. The green point lies outside the influence distance of the steam injection and shows little to no change. The P50 (solid, bold) result of the yellow point moves to more stable conditions. Note the different ranges between the P10- P90 pairs (dashed lines), where, e.g., a much larger uncertainty is present in the red curves compared to the blue curves.

The four probed locations in Figure 4 show significantly different results. Two of the sampled points show a trend of Tau Ratio (P50) that exceeds the critical limit of 1.0. Point 1 shows the most critical values. The uncertainty range of point 1 is however noticeably smaller compared the range from point 4. The time series of point 3 - located at some distance from the stream injection - remains constant through the time series whereas point 2 becomes more stable over time.

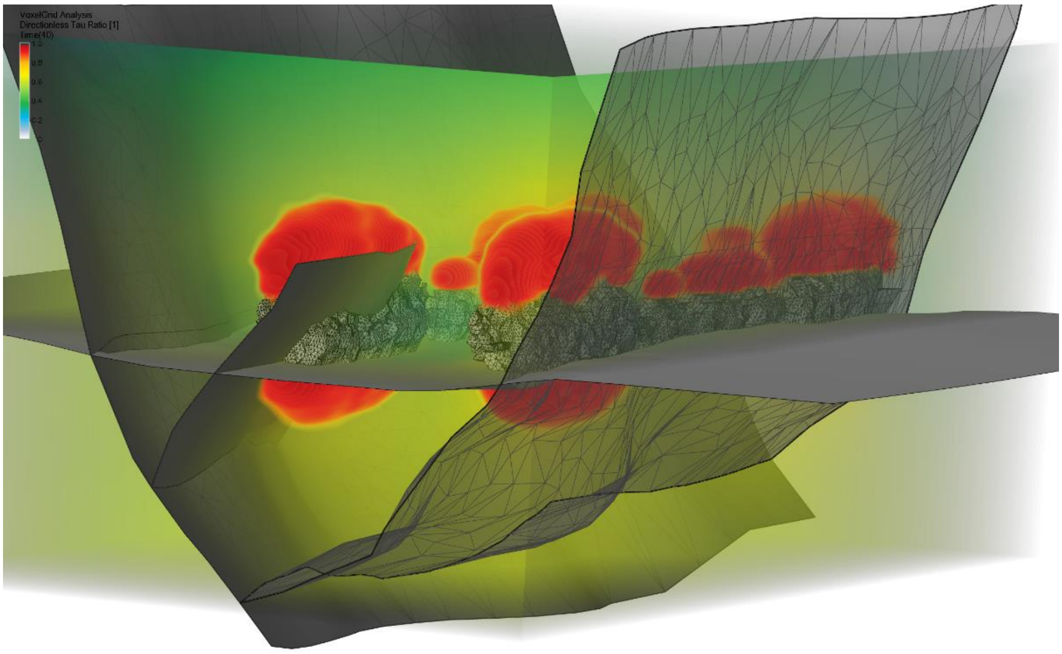

Figure 5 – Volume rendering of the directionless Tau Ratio in which the critical values are shown as opaque red clouds. The critical sections are located directly above and below the temperature bodies (Last time step in analysis, temperature body is rendered as reference).

In order to understand the results in more detail and also assess the sub-seismic fractures which may be present, we perform a volume operation on the geomechanical 3D mesh directly, which is explained in detail in Ansari et al (2012) and Holland (2015). We use the effective stress tensor from the Abaqus simulation to calculate Tau Ratio for the most critical fault or fracture orientation possible. This conservative approach reveals whether the worst-case fault orientation would yield critical conditions. As no observed fault orientations are needed for this calculation, the analysis can be applied to the entire stress volume and can be rendered accordingly (Figure 5).

The volume rendering of the results shows that potentially critically stressed conditions are present below and above the steam injection, rendered in Figure 5 as opaque red clouds. The growth of the clouds coincides primarily with rising temperatures in the direct vicinity of the steam injection and less with the pore pressure changes. The critical volume extends upwards into the impermeable cap rock. We further investigate the cap rock integrity by extracting the maximum tau ratio over the entire time series from the mesh at the interface between the cap rock and the reservoir (Figure 6). The critical areas are located directly above the steam injection bodies. The two lower hemisphere plots give an indication of the fracture orientations which would yield critical values at these locations, where red sections in the lower hemisphere plots reveal the fracture orientations which would be critically stressed. The two locations probed show that a wide range of fracture or fault orientations are potentially critically stressed. Despite their close proximity (30 m), the critical orientations of fracture poles differ significantly between the two stereo plots.

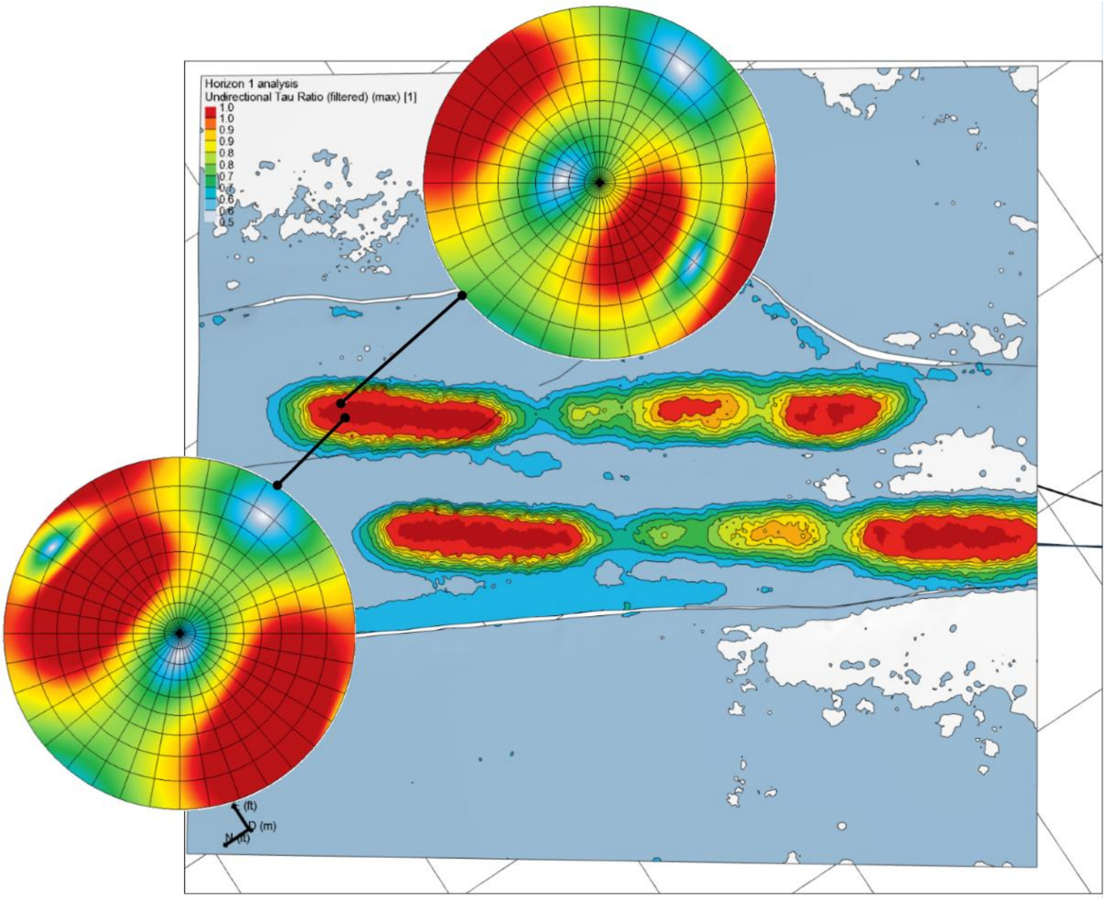

Figure 6 – Map view of the most critical Tau Ratio values of the time series extracted at boundary between the cap rock and reservoir. Areas that could have critically stressed fractures are rendered in red. For two locations, lower hemisphere plots are drawn which highlight the critical fracture or fault orientations (Lower hemisphere stereo plots show critical orientations of fracture poles).

4. Discussion

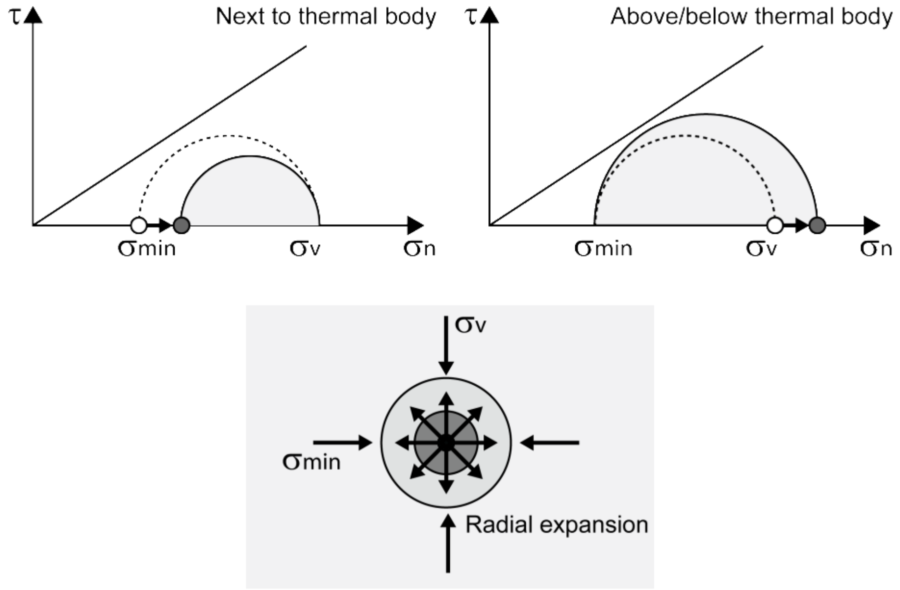

Figure 7 – Sketch of the changes in the stress conditions above and at the sides of the radially expanding temperature body. At the sides, the expansion increases the minimum horizontal stress component, making the Mohr Circle smaller. Above and below, the thermally induced stresses increase the vertical stress component, making the Mohr Circle larger.

Stress perturbations in the presented SAGD scenario are a result of the thermal expansion of the rock in response to the steam injection. The displacement caused by the injection happens radially around the sub-horizontal wellbores and reaches displacements of approximately 10 cm in the sub-surface, and 2 cm at the surface (Holland, 2015). The stress field perturbations are confined to the proximity of the steam injection. Fault surfaces in close proximity to the injection sites become critically stressed and potentially shearing early in the time series, presenting a risk for loss of the lateral seal integrity (Figure 3, Figure 4). As these faults partly extend into the impermeable cap-rock, a slip event in this scenario may also lead to vertical fluid migration (Figure 1). An assessment of the worst-case fracture stability reveals the critical volumes in which a potential for fracture activation exists (Figure 5). The critical volumes are located above and beneath the steam injection. This pattern is related to the stress perturbation of thermal expansion of the rock within the present stress field.

In this scenario, the well trajectories are drilled in the direction of the maximum horizontal stress S_{Hmax} (Table 2). The thermal expansion causes the thermally induced stresses to act radially around the well bore. Above and below the well bore, the changes primarily increase the vertical stress, whereas laterally the minimum horizontal stress is increased. As the minimum horizontal stress is approximately the minimum principal stress and the vertical stress the maximum principal stress, a Mohr Circle (Jung, 1946/1947) for a location left or right of the steam injection would shrink in diameter. A Mohr Circle on top or below would increase in diameter (Figure 7).

The stress perturbations are acting locally, but the volume of the potentially critically stressed fractures extends vertically into the cap-rock (Figure 5), and the critical area can be mapped onto the interface between the reservoir and cap-rock (Figure 6). Here a detailed fracture assessment should be carried out to rule out the possibility of the existence of critically oriented fractures. Due to the radial expansion of the rock around the steam injection well bores and the interaction of the two injection sites, the critical fracture orientations change with location (Figure 6).

5. Conclusion

Subsurface operations where significant changes in temperature or pressure are expected are likely to experience local perturbations of the stress conditions. This was demonstrated on a SAGD scenario in which the thermal expansion caused by the injection of steam leads to the changes. For a risk assessment, the results of a reservoir simulation can be used to feed into a geomechanical simulation of the subsurface system. Due to the fundamentally different simulation meshes and different properties and requirements of the simulations and meshes, an integration platform is required which enables the construction and population of the anticipated 3D mesh for the geomechanical simulation. The required extension in size as well as the population of the model (with properties which are typically available as a well-centric 1D geomechanical model) are carried out in JewelSuite™. Here also a structural model is constructed based on triangulated surfaces.

Enforced gradients in the triangle size of these surfaces are used to constrain the tetrahedron sizes of the Abaqus mesh. Using a linear-elastic material model, a one-way coupling is used where we provide the temperature and pore pressure evolution as boundary conditions to the Abaqus/Standard solver. The post-processing of the results is done in the JewelSuite™ subsurface modeling software to provide for the application of specialized geomechanical probing and analysis tools.

Upon the identification of critically stressed fractures, locations and time steps, purpose made tools help the user to identify fracture orientations with high risk.

6. Acknowledgement

The authors like to thank Baker Hughes Inc. management for permission to publish this article.

7. References

Ansari, S. et al., 2012. Caprock Integrity Case Study for Non-thermal Polymer Flooding Project Using 4D Reservoir Coupled Geomechanial Simulation. *SPE Heavy Oil Conference, Calgary/Canada,* SPE (157912).

Barton, C. A. & Zoback, M. D., 1995. Fluid flow along potentially active faults in crystalline rock. *Geology,* 15(5), pp. 467-470.

Butler, R. M., 1991. *Thermal recovery of oil and bitumen.* Englewood Cliffs, N.J.: Prentice Hall.

Byerlee, J. D., 1978. Friction of rock. *Pure & Applied Geophysics,* Volume 116, pp. 615-626.

Chou, P. C. & Pagano, N. J., 1967. *Elasticity - Tensor, Dyadic, and Engineering Approaches.* Princeton, N.J.: Van Nostrand.

ERCB, 2010. *Total E&P Canada Ltd.Surface Steam Release of May 18, 2006, Joslyn Creek SAGD Thermal operation,* Alberta: Energy Resources Conservation Board.

ERCB, 2013. *Primrose East Bitumen Emulsion Release, January 3, 2009,* Alberta: Energy Resources Conservation Board.

Gu, F., Chan, M. Y. & Fryk, R., 2011. Geomechanical-Data Acquisition, Monitoring and Applications in SAGD. *Journal of Canadian Petroleum Technology,* 50(6), pp. 9 - 21.

Holland, M., 2015. Directionless Fracture Stability Assessment based on a 4-D Geomechanical Model of a SAGD scenario. *First Break,* 33(3), pp. 47-52.

Holland, M. et al., 2010. *Value of 3D Geomechanical Modeling in Field Development - A new Approach using Geostatistics.* Al-Khobar, Society of Petroleum Engineers.

Jung, F., 1946/1947. Der Culmannsche und der Mohrsche Kreis. *Österreichisches Ingenieur-Archiv,* 1(4-5), pp. 408-410.

van der Zee, W., Ozan, C., Brudy, M. & Holland, M., 2011. *3D Geomechanical Modeling of Complex Salt Structures.* Barcelona, SIMULIA Customer Conference.

van der Zee, W., Plug, W.-J., Niewland, D. & Holland, M., 2014. *Geomechanical Optimization of Underground Gas Storage Operation.* Providence, SIMULIA Community Conference.

Zoback, M. D., 2007. *Reservoir Geomechanics.* Cambridge: Cambridge University Press.

8. Appendix

The SAGD scenario used in this publication is synthetic. Although closely aligned to a realistic scenario, the structural model, the positioning of the reservoir grids, the external stress field as well as the geomechanical properties are fictional.

Table 1 – Material properties used in the analysis per element set.

Element sets	Top horizon	Density (kg/m^3)	Young's modulus (GPa)	Poisson's ratio	Thermal expansion coefficient (K^{-1})
Top	Topography	2,200	3.0	0.3	-
Layer 1	Horizon 1	2,250	1.5	0.25	$3 \cdot 10^{-5}$
Layer 2	Horizon 2	2,270	2.7	0.27	$3 \cdot 10^{-5}$
Layer 3	Horizon 3	2,310	1.2	0.26	$3 \cdot 10^{-5}$
Layer 4	Horizon 4	2,350	1.0	0.27	$3 \cdot 10^{-5}$
Base	Horizon 5	2,390	1.5	0.3	$3 \cdot 10^{-5}$

Table 2 – Parameters for initial stress field.

Property	Value
Effective Stress Ratio Sh_{min} at surface	0.7
Effective Stress Ratio Sh_{min} at 280 m TVD	0.5
Effective Stress Ratio SH_{max} at surface	0.9
Effective Stress Ratio SH_{max} at 280 m TVD	0.7
Azimuth of SH_{max}	35 DEG